

Article

Silicon Kerf Recovery via Acid Leaching Followed by Melting at Elevated Temperatures

Tinotenda Mubaiwa ^{1,*}, Askh Garshol ¹, Alexander Azarov ²  and Jafar Safarian ¹ 

¹ Department of Materials Science and Engineering, Norwegian University of Science and Technology, N-7491 Trondheim, Norway; askhg@ntnu.no (A.G.); jafar.safarian@ntnu.no (J.S.)

² Department of Physics, Centre for Materials Science and Nanotechnology, University of Oslo, P.O. Box 1048 Blindern, N-0316 Oslo, Norway; alexander.azarov@smn.uio.no

* Correspondence: tinotenda.mubaiwa@ntnu.no; Tel.: +47-92540411

Abstract: The aim of this work was to study the purification of silicon kerf loss waste (KLW) by a combination of single-acid leaching followed by inductive melting at high temperatures with an addition of fluidized bed reactor (FBR) silicon granules. The KLW indicated an average particle size (D₅₀) of approximately 1.6 μm, and a BET surface area of 30.4 m²/g. Acid leaching by 1 M HCl indicated significant removal of impurities such as Ni (77%), Fe (91%) and P (75%). The combined two-stage treatment resulted in significant removal of the major impurities: Al (78%), Ni (79%), Ca (85%), P (92%) and Fe (99%). The general material loss during melting decreased with an increasing amount of FBR silicon granules which aided in the melting process and indicated better melting. It was observed that the melting behavior of the samples improved as the temperature increased, with complete melting being observed throughout the crucibles at the highest temperature (1800 °C) used, even without any additives. At lower temperatures (1600 °C–1700 °C) and lower FBR-Si (<30 wt.%) additions, the melting was incomplete, with patches of molten silicon and a lot of surface oxidation as confirmed by both visual observation and electron microscopy. In addition, it was indicated that more reactive and volatile elements (Ga, Mg and P) compared to silicon are partially removed in the melting process (51–87%), while the less reactive elements end up in the final silicon melt. It was concluded that if optimized, the combined treatment of single-acid leaching and inductive melting with the addition of granular FBR silicon has great potential for the recycling of KLW to solar cells and similar applications. Moreover, the application of higher melting temperatures is accompanied by a higher silicon yield of the process, and the involved mechanisms are presented.



Citation: Mubaiwa, T.; Garshol, A.; Azarov, A.; Safarian, J. Silicon Kerf Recovery via Acid Leaching Followed by Melting at Elevated Temperatures. *Recycling* **2024**, *9*, 66. <https://doi.org/10.3390/recycling9040066>

Academic Editors: Sossio Fabio Graziano, Rossana Bellopede, Giovanna Antonella Dino and Nicola Careddu

Received: 17 June 2024

Revised: 28 July 2024

Accepted: 5 August 2024

Published: 8 August 2024



Copyright: © 2024 by the authors. Licensee MDPI, Basel, Switzerland. This article is an open access article distributed under the terms and conditions of the Creative Commons Attribution (CC BY) license (<https://creativecommons.org/licenses/by/4.0/>).

1. Introduction

As the world moves towards clean and sustainable energy away from fossil fuels, solar energy has played a key role as a source of clean energy and its use has grown quite significantly over the past few decades, with several technologies being currently employed in the production of solar grade silicon [1–9]. Silicon production from secondary sources (recycling) has been proven to be an even cleaner and more environmentally friend route when compared with silicon production from primary sources. One such option is the recycling of kerf loss waste (KLW), which accounts for over 30% of material loss during the silicon wafer cutting process [10–12]. Applying the modern diamond-coated steel wires for the slicing process of silicon ingots introduces some impurities to the KLW, and these include polymer material and Al from the sacrificial and mounting beams, some C from glue joint and lubricants (whose main component is polyethylene glycol (PEG) with average molar mass of around 400 g or a combination of PEG and diethylene glycol (DEG)), Fe and Ni from the nickel electroplated diamond cutting steel wire as shown in Figure 1 [13,14].

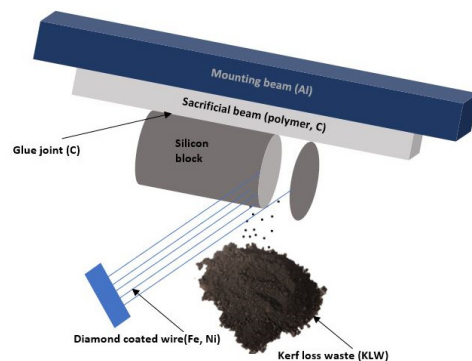


Figure 1. Illustration of the wafer slicing process and impurity sources.

The main slicing techniques are loose abrasive sawing (LAS) and diamond wire sawing (DWS). The DWS method has gradually replaced the LAS method due to its superior performance and less damage to the surface of the ingot. The recycled KLW has several uses at present, including catalysis, hydrogen generation, lithium-ion batteries, ceramics, alloying and high purity Si, among other uses. Several methods can be used for recycling KLW, especially acid leaching and metallurgical processes or a combination of the two. The direct reintroduction of KLW back into the crystalline silicon production for photovoltaics is problematic due to the strict purity requirements of at least 6 N purity in the photovoltaics industry [15–18]. At present, researchers are trying to find the most scientific, environmentally friendly and economically viable method for recycling KLW into useful products. Halvorsen et al. applied a combination of melting, hot pressing, plasma spray and further purification to produce 2–4 N silicon at pilot and industrial scales in 2017 [19]. In 2018, Kong et al. used acid leaching, pelletizing and inductive melting and produced 4 N ingots at lab scale. Yang et al. combined acid leaching, calcination ($500\text{ }^{\circ}\text{C}$) and high temperature vacuum deoxidation ($900\text{ }^{\circ}\text{C}$) as well as slip casting and produced 5 N silicon for Si_3N_4 crucibles at lab scale [14]. In 2020, Kong et al. used pelletizing and vacuum refining, combining crystallization and refining in one step to produce 2 N silicon at lab scale [20]. They also studied the melting and impurity removal mechanism. In 2016, REC solar successfully managed at pilot scale and in 2020 they moved to full scale industrial recycling of kerf to solar grade silicon [21]. Recently, Bao et al. [22] examined the refractory behavior of acid-leached KLW during melting and the effect of oxygen content on the overall melting behavior in a vacuum induction furnace, while the current study looks at the effect of blending KLW with lumpy silicon in an open-air induction furnace purged with argon gas. Thus, this study explores the combination of single-acid leaching followed by inductive melting and the addition of lumpy pure (fluidized bed reactor) silicon to aid the melting process of the KLW, which to the best of our knowledge has not yet been implemented, as shown in Figure 2. The use of FBR granules (which are produced by a less energy intensive and environmentally friendlier process) in the melting of KLW presents practical opportunities on the melting process as well as dilution of trace impurities. The acid leaching mainly targets the metallic impurities as well as P, while inductive melting is responsible for carbonic and volatile compound elimination. Silicon kerf recycling is still a developing field and there are still a lot of challenges and room for optimization and improvement.

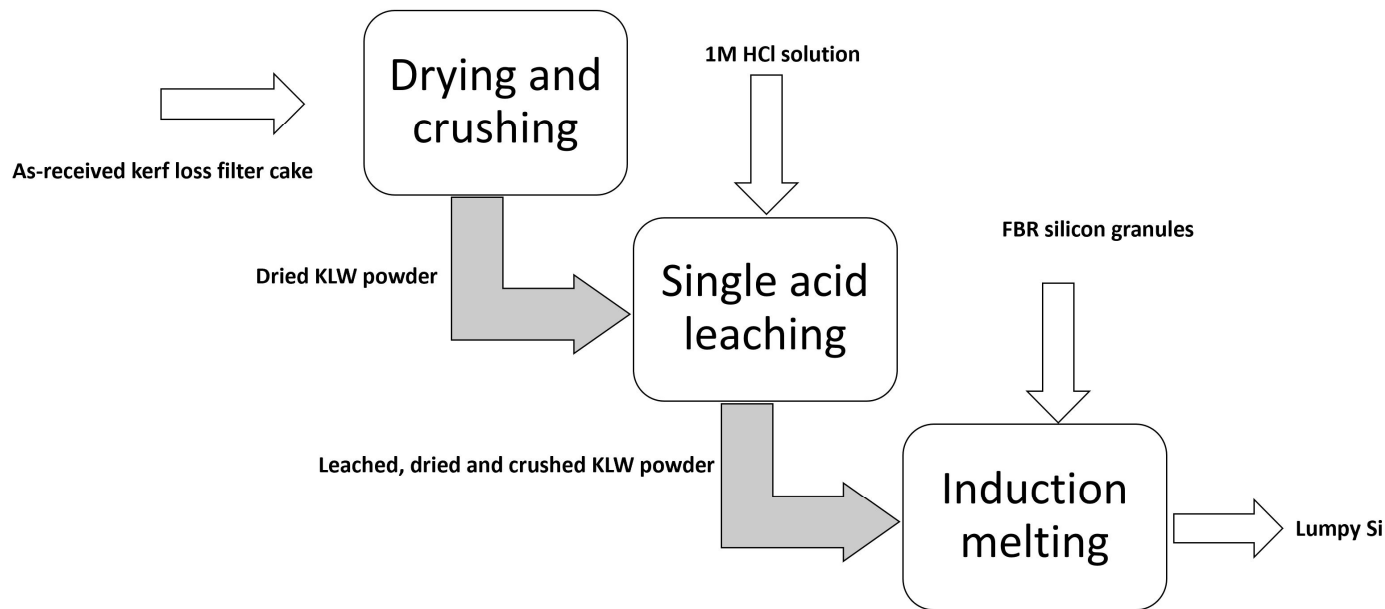


Figure 2. Flowsheet for experimental silicon–KLW recycling in this study.

2. Materials and Methods

2.1. Materials

A Si kerf sample was received in cake form from an industrial supplier with approximately 45% moisture content. This is after it has already been separated from the cutting fluid. It was dried for 24 h at 80 °C to remove the absorbed moisture. After drying, the kerf sample was manually deagglomerated by hammering before characterization and further use.

2.2. Leaching

The dried deagglomerated Si kerf was leached with 1 M concentration of HCl at 40 °C for 1 h using a jacketed glass reactor with a mechanical stirrer as shown in Figure 3. The solid/liquid ratio in leaching was 1:10. For the leaching process, 100 g samples were used in a 1 L leaching reactor. The silicon particles were then separated using a lab scale centrifuge at 4200 rpm. We chose centrifugation after trying vacuum filtration with filter paper which was ineffective due to the sticky nature of the kerf mud. The solid residue was washed by distilled water on a hot plate at 25 °C for 30 min, twice, and centrifuged and dried in an oven at 80 °C for 24 h. This process was repeated several times to have enough material for further melting trials, and three leached samples were characterized, and the average compositions were determined.

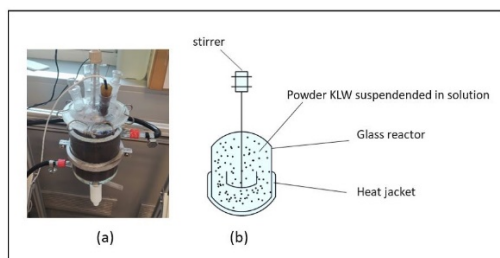


Figure 3. Leaching setup used for acid leaching purification—(a) actual and (b) schematic.

2.3. Melting

After leaching and drying, the Si kerf was melted using an induction furnace, with 75 kW power at targeted temperatures between 1600 °C and 1800 °C. The samples were charged into graphite crucibles with 4.2 cm inner diameter, 5 cm outer diameter and 18 cm

height. The graphite crucibles had graphite lids. To make the charged kerf more compact, the KLW powder samples were compressed. The crucibles were put in a closed chamber, while an Ar flow was maintained to prevent oxidation of silicon and crucible containers. The Si kerf powder was initially melted without any additives, and fluidized bed reactor (FBR) silicon granules were also added in different proportions up to 40 wt.%. The FBR polysilicon granules, which are of very high purity, act as ‘seed’ material for the melting of KLW while at the same time not introducing contaminants due to their high purity. The holding time was 1 and 2 h, with slow cooling afterwards in the furnace. After cooling to room temperature, the crucibles were cut from the middle vertically by a diamond blade and were evaluated, and metallography samples were prepared from the intersections. Figure 4 shows the experimental setup. It must be noted that the furnace set-up for our conditions was semi-open as smaller crucibles were placed inside a bigger crucible with continuous circulation of argon gas.

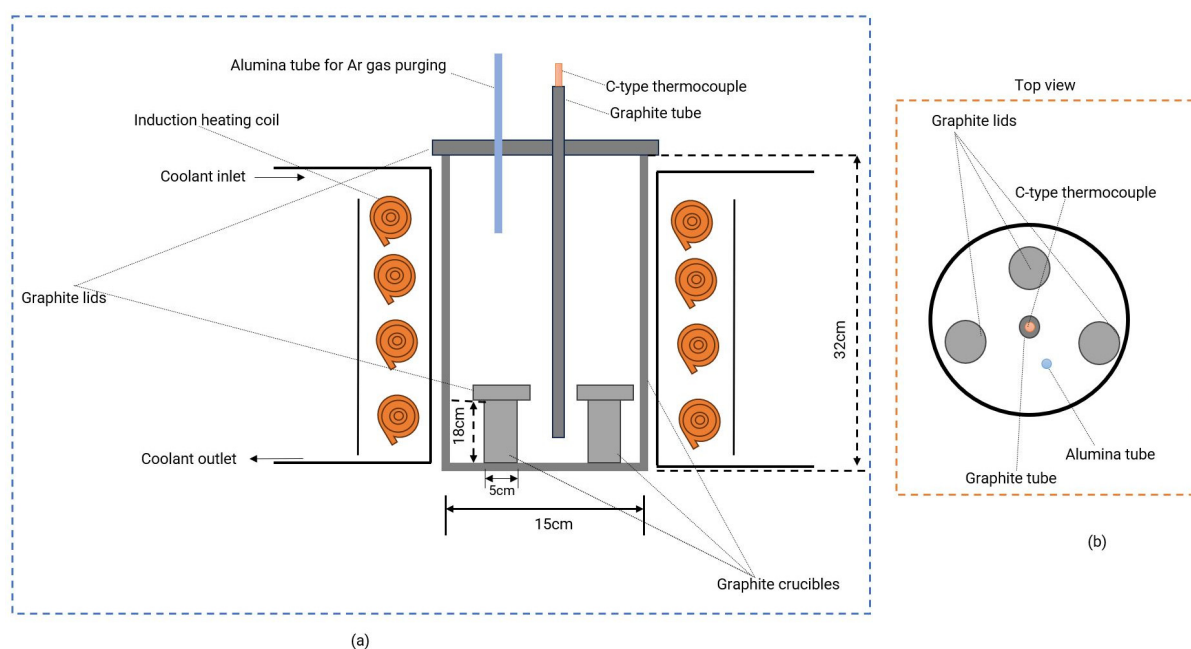


Figure 4. Experimental setup (a) and the top view (b).

2.4. Characterization

The as-received Si kerf samples were characterized by glow discharge mass spectrometry (GDMS) to analyze elemental compositions before and after each treatment, scanning electron microscopy (SEM) for analysis of the morphology, Brunauer–Emmett–Teller (BET) method for surface area measurement, infrared absorption and non-dispersive infrared detection (LECO) method to measure combustion gases within the kerf and particle size distribution (PSD) analysis. After melting, the samples were characterized by scanning electron microscopy (SEM), secondary-ion mass spectrometry (SIMS), and glow discharge mass spectrometry (GDMS).

Sample Preparations

For GDMS, we used both powder and lumpy solid samples. Powder samples were ground after drying (before and after leaching), while solid samples were cut by a diamond blade and polished to produce a flat surface. SEM was conducted on powder (as-received) samples after drying, as well as solid samples after melting. The solid samples were placed in epoxy resin and polished until a flat shiny surface was produced and then coated with carbon powder for analysis. LECO, BET and PSD analyses were also conducted on dried and ground powders, whilst SIMS was conducted on polished samples cut using a rotating diamond blade.

3. Results and Discussion

In this study, we propose a recycling route using a combination of single-acid (HCl) leaching with inductive melting of powder KLW with the addition of granular FBR silicon. The efficiency of the combined treatment was evaluated and the melting behavior of the silicon powder with and without additives was studied. The effect of different holding temperatures was also studied to find the optimum conditions.

3.1. Characterization of As-Received KLW

The particle size distribution showed an average particle size (D_{50}) of approximately $1.6 \mu\text{m}$, indicating that the KLW consists of very fine material, which makes it prone to oxidation and presents difficulties in handling and storage. The BET surface area was $30.4 \text{ m}^2/\text{g}$, which is also a very high surface area, showing that the cutting technology during the wafering process has generally improved over the years. The SEM micrographs in Figure 5 showed the typical flakes of loose agglomerates of impurities distributed inside the main silicon particles pack, consistent with KLW particles.

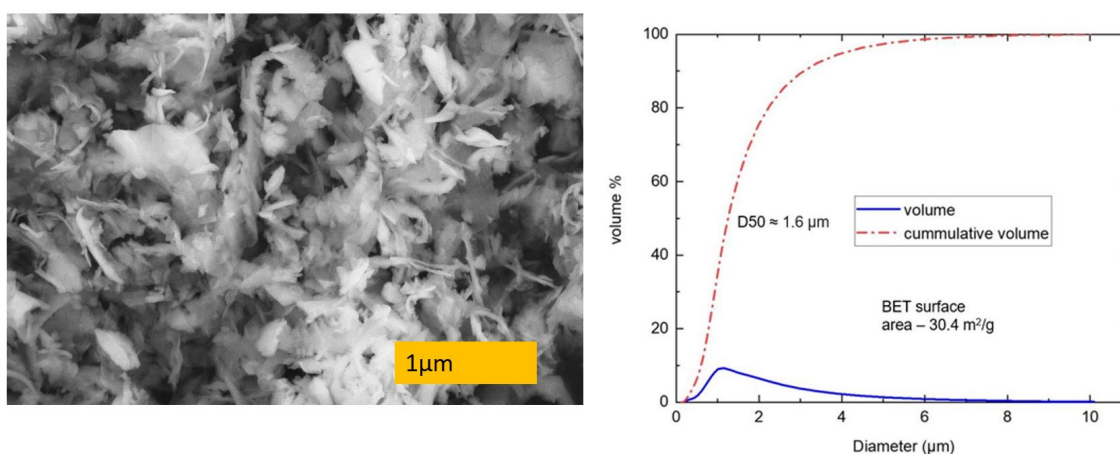


Figure 5. Secondary electron SEM image of Si kerf (left), and particle size distribution and BET surface area (right).

Inspecting the silicon kerf sample using SEM reveals that the particles are flakes with a small width and thickness, in nano scale. This may be due to the abrasion via tiny diamond particles and the brittleness of silicon. This geometry of the particles gives the high measured specific surface area seen in Figure 5. The SEM image shows that the thickness of many particles is below 100 nm, and hence the material can be considered a nanomaterial.

3.2. Elemental Composition Changes

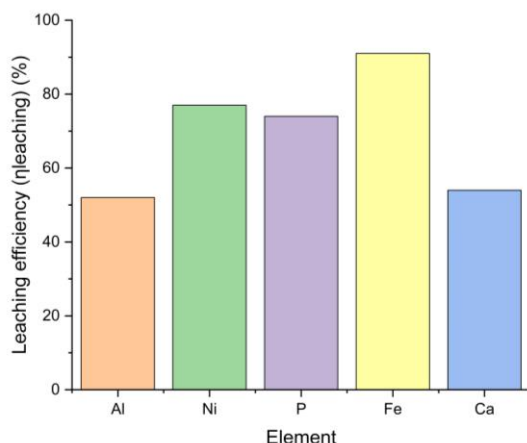
The elemental compositions were measured using GDMS to evaluate the effectiveness of the different combined treatments. Table 1 shows the initial as-received chemical composition and the compositions after leaching by HCl and after melting at different temperatures and different FBR silicon additions.

Table 1. Elemental composition in ppmw.

Element	Al	B	Ca	Cu	Fe	Ga	Mg	Mn	Ni	P	Ti
Initial	11,000	0.44	37.9	2.1	195.9	5.2	5.0	2.5	169.6	9.8	5.6
After leaching	5270	1.9	17.3	2.8	18.3	1.9	2.73	1.0	39.7	2.5	2.2
Leaching + 1600 °C (40 wt.% FBR)	763	0.16	1.6	1.9	2.9	1.4	0.51	1.5	40.2	0.52	1.8
Leaching + 1700 °C (40 wt.% FBR)	1620	0.57	4.5	1.6	6.6	0.82	0.73	4.1	39.5	1.02	1.9
Leaching + 1800 °C (40 wt.% FBR)	2410	0.23	1.7	1.05	9.1	0.47	0.22	1.2	35.7	0.74	1.66

3.2.1. The Effect of Leaching Pretreatment

The effect of leaching as a pretreatment step under moderate conditions of concentration, temperature and residence time were evaluated and here the results are presented. After leaching with 1 M HCl at 40 °C for 1 h and a liquid/solid ratio of 10:1, the removal efficiencies (η_{leaching}) for Al, Ni, P, Ca and Fe (the target impurities during leaching treatment) were 52%, 77%, 74%, 54% and 91%, respectively, and are presented in Figure 6.

**Figure 6.** Leaching efficiencies of the different elements after leaching pretreatment step.

These numbers were obtained using the following formula in Equation (1):

$$\eta_{\text{leaching}} = C_i - C_{f,\text{leaching}} / C_i \times 100 \quad (1)$$

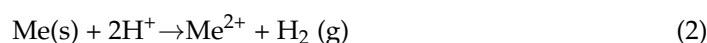
where C_i is the composition of element i before acid leaching and $C_{f,\text{leaching}}$ is the composition of element i after acid leaching. The leaching pretreatment conditions were effective for the reduction of Fe while moderate for Ni and P and relatively low for Al and Ca. The high amount of Al (approximately 1 wt.%) was responsible for the relatively low metallic impurity removal at lower acid concentrations (1 M), coupled with the lower residence time of 1 h, as Al removal strongly depends on acid concentration (up to 4 M concentration) and residence time [23]. The reason for the moderately lower acid concentration and temperature in this study is to cater for typical industrial applications where reagents and energy consumption are major cost drivers. The leaching efficiencies were, however, still within acceptable values as a pretreatment step before pyrometallurgical treatment.

The liquid/solid ratio has been optimized by several researchers, and it is widely accepted that 10:1 is an optimum for the leaching process of KLW in terms of both reagent consumption and leaching efficiency. The Ni removal efficiency (77%) under these conditions was quite good considering the fact that Yang et al. (2020) got approximately 84% Ni removal at optimum conditions of 4 mol/L HCl concentration, 60 °C temperature and 3 h. According to Yang et al. (2019), to obtain around 95% Al recovery, the optimum leaching

conditions are 4 M HCl, 3 h leaching time and a liquid/solid ratio of 10 at a temperature of 60 °C. In our case, replicating these conditions only gave an Al removal efficiency of about 65%, meaning those conditions were not enough for the relatively high Al content of approximately 1.1 wt.% compared to the 0.77 wt.% used by Yang et al.

3.2.2. The Dissolution Mechanism of Impurities during Leaching of KLW Powder

The general reaction for the dissolution of metallic impurities in KLW such as Ni, Fe, Ca, Mg etc. in acidic media can be represented by Equation (2):



where Me represents the metallic elements. A shrinking particle model can be assumed for the dissolution reaction as shown in Figure 7 [24–26].

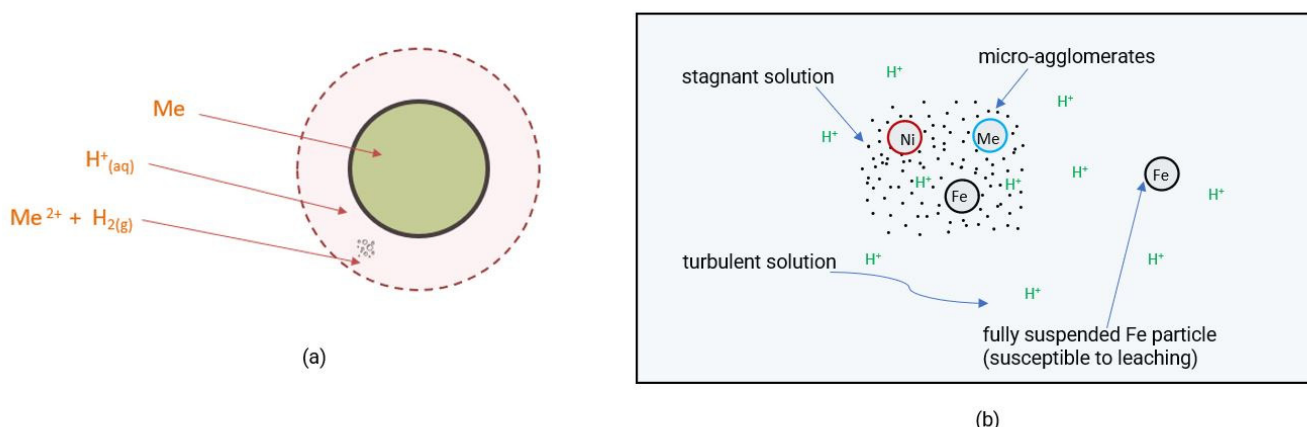


Figure 7. Physical model for impurity dissolution in acidic media (a) and micro agglomeration of solid particles (b).

In principle, the dissolution of metallic impurities such as Ni and Fe in acidic solutions is fast and an incomplete dissolution of these impurities even when significantly high volume of solutions is used may be attributed to improper contact of the solution with these particles. We may propose that since the sample has many fine particles, they may form tiny agglomerates during the leaching, and hence non-ideal suspension occurs. In ideal or full suspension, we have no physical contact of the suspended solid particles that causes perfect contact of the whole particle surface with the solution (Figure 7b). However, in non-ideal suspension, there is not complete contact of the solid particle with the solution, and hence the solid/liquid reaction interfacial area is reduced. If the agglomeration of particles occurs, this reaction surface is more reduced. Moreover, the agglomeration of particles during leaching reduces the rate of digestion of metallic particles as the particle is in contact with a stagnant solution, or in other words not enough moving solution, and hence mass transport of the solution to the surface of the metal particle may be a rate-limiting step as shown in Figure 7b. Regarding the presented schematic in Figure 7b, we may say that the mass transport of H^+ is limited due to micro-agglomerate formation in the system. For the practical application of leaching as a pretreatment step for KLW powder, which is very fine and prone to agglomeration, it is therefore important to optimize the reactor vessel geometry, agitation and residence time. Additionally, periodic application of ultrasound pulses can mitigate the effects of agglomeration.

3.2.3. The Effect of Induction Melting and the Behavior of Impurities at Elevated Temperatures

The effect of induction melting with the use of FBR silicon granules to gain insights on the role played by FBR silicon addition with regards to the reduction of impurities was

evaluated. If we consider only removal degree during the melting, taking the leached sample as the feed, we can evaluate the impurity removal efficiency using Equation (3):

$$\eta_{\text{melting}} = (1 - C_{f,\text{melting}}(m_{\text{Si-Kerf}} + m_{\text{Si-FBR}})/(C_{f,\text{leaching}} \cdot m_{\text{Si-Kerf}})) \times 100 \quad (3)$$

where $C_{f,\text{leaching}}$ is the composition after leaching, $m_{\text{Si-Kerf}}$ is the mass of the leached powder KLW, $m_{\text{Si-FBR}}$ is the mass of lumpy pure silicon and $C_{f,\text{melting}}$ is the composition after melting. The highest removal efficiencies for the different temperature conditions studied (obtained at 1600 °C) during melting, (η_{melting}), was 76%, 85%, 74% and 65% for Al, Ca, Fe and P, respectively, while it was negative for Ni, indicating no effect during melting. For Ga and Mg, this was achieved at 1800 °C with efficiencies of 59% and 87%, respectively. It was observed that Ni is not affected by the inductive melting treatment and maintains pretty much the same composition as the one after the leaching treatment. The other impurity elements decreased in composition after the inductive melting. Based on these results in the melting step and the characteristics of the impurities, we can evaluate the behavior of the impurities by classifying them into three groups as follows:

1. Relatively more reactive elements than Si (Al, Ca, Mg and Ti):

As can be seen in Table 1, the values of these elements decrease after inductive melting at all of the studied temperatures. Al and Ca are mostly removed to an oxide phase during the melting. The elements are distributed mostly to an adjacent slag that contains Si, Al, Ca and Mg. In this case, the overall slag formation reaction can be written as shown in Equation (4):



Obviously, the melting points of the slag forming components are high and exceed 1700 °C, in which SiO_2 gets molten. Hence, the slag formation is dependent on diffusion and melting time. Therefore, it is expected that the formation of the slag and separation is better at higher temperatures and hence the single-phase liquid phase is formed when higher temperatures are applied for melting.

2. Volatile elements (Ga, Mg and P):

The composition of Ga, Mg and P is lower after melting than their concentrations in the leached silicon mostly due to their volatility, and hence their loss is observed when melting at elevated temperatures. These elements are more volatile compared to Si and are mostly distributed into the gas phase; the vapor pressures of these elements were studied before, and the principles applied in vacuum refining are valid in the present experimental work [17–28].

3. Less reactive elements than Si (Cu, Fe and Ni):

These elements are mostly unaffected by the inductive melting and the observed lower concentrations are mainly due to the dilution via FBR silicon addition, as we observe lower concentration of these elements when more FBR is added (Table 1).

Less reactive metals than silicon such as Cu, Fe and Ni are stable in contact with molten silicon and hence they are easily getting dissolved in liquid silicon and their oxidation does not occur, as conversion to their oxides (by SiO_2) is not possible thermodynamically. It is worth noting that these elements have low concentrations and hence they are in very dilute concentrations and their corresponding very low chemical activities allow them to maintain their elemental forms and dissolve in the liquid silicon. An additional treatment step like directional solidification is expected to further reduce most of these impurities and attain solar-grade acceptable concentrations.

3.2.4. The Combined Effect of Leaching and Induction Melting

After discussing the individual steps, we evaluated the combined effect of the two-stage process on the overall impurity removal efficiencies and the purity of the lumpy

silicon blocks produced. After leaching and induction melting at 1600 °C with the addition of 40 wt.% FBR, the overall removal efficiencies ($\eta_{\text{leaching+melting}}$) of Al, Ni, Ca, P and Fe were 93%, 76%, 96%, 96% and 99%, respectively. These numbers were calculated using Equation (5):

$$\eta_{\text{leaching+melting}} = C_i - C_{f,\text{melting}}/C_i \times 100 \quad (5)$$

where C_i is the initial composition before leaching and $C_{f,\text{melting}}$ is the final composition after both treatments. After a combination of leaching and induction melting at 1700 °C with the addition of 40 wt.% FBR, the removal efficiencies ($\eta_{\text{leaching+melting}}$) of Al, Ni, Ca, P and Fe were 85%, 77%, 88%, 90% and 97%, respectively. For the same treatment at 1800 °C, the removal efficiencies of Al, Ni, Ca, P and Fe were 78%, 79%, 96%, 92% and 95%, respectively. Comparing the results at 1700 °C and 1800 °C, it can be seen that there is not much difference between the two temperatures, and there may be no incentive to go to temperatures higher than 1700 °C. Figure 8 summarizes the combined effect of the different conditions applied in this study.

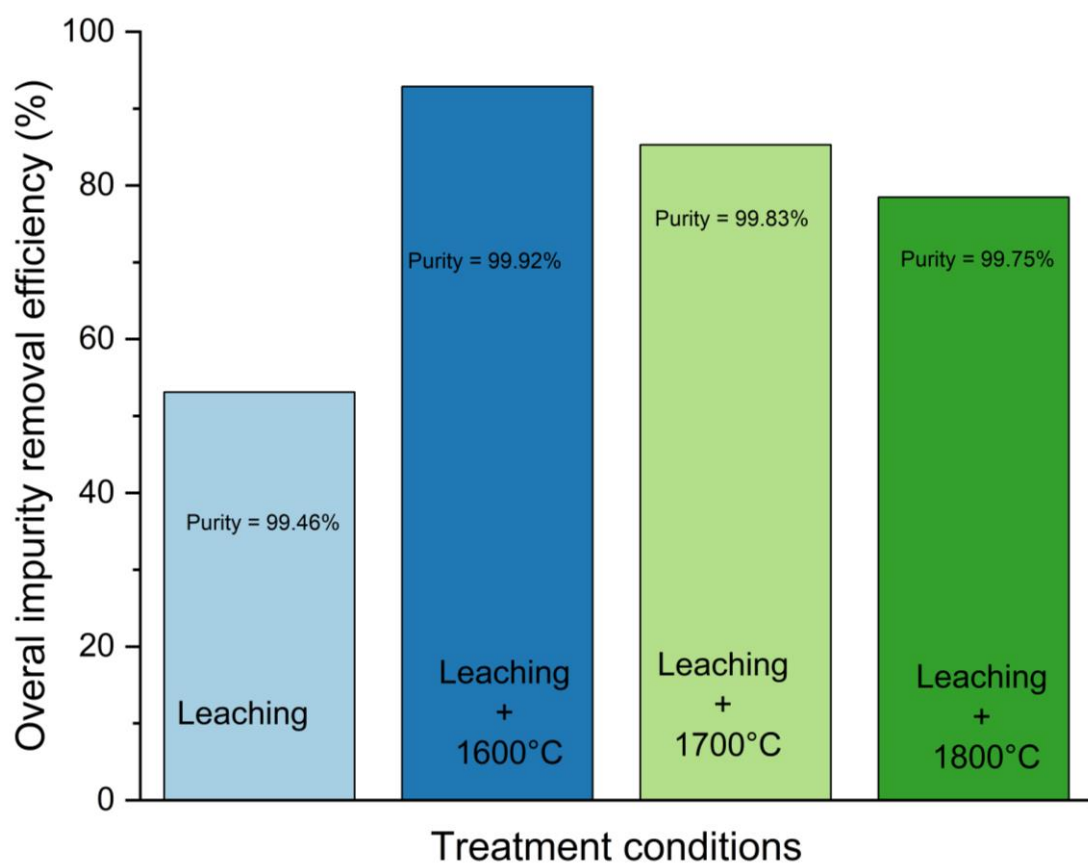


Figure 8. Combined effects of leaching and induction melting under different conditions.

The main challenges in recycling KLW are melting the material and removing the metallic impurities, and hence the combination of acid leaching and high temperature melting was applied in this research. The use of FBR silicon granules was to improve the melting step as these granules have no surface oxide layer, which usually covers the KLW particles and slows down the melting process via a thin oxide layer barrier. As a result, we observed that the addition of FBR silicon granules improves the melting, which is mostly due to the better/faster melting than the fine particles and the formation of initial molten droplets which enhances the melting phenomenon. The successful mix of the two solar silicon materials for KLW recycling at the lower applied melting temperatures of this study is of practical importance, as the processing time can be decreased and hence the production rate can be improved prior to silicon ingot casting.

3.3. Mass Changes and Si Recovery during Melting

The melting of KLW at elevated temperatures is accompanied by material loss, since it contains some moisture as well as organic and volatile material, as evidenced by the losses presented in Figure 9.

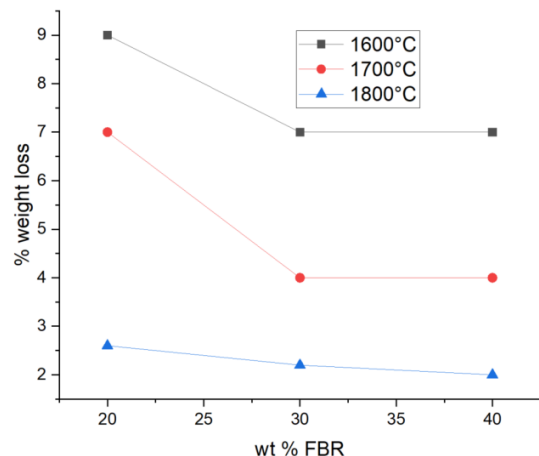


Figure 9. Mass changes during melting with different FBR additions.

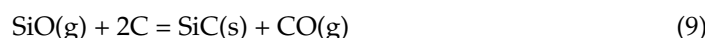
The general mass loss was between 2 wt.% and 10 wt.% and decreased with an increasing amount of FBR silicon granules, which aided in the melting process and gave better melting. It was observed that at 30 wt.% and beyond, the general weight loss is negligible; hence, there is no need for further addition of FBR-Si granules beyond this limit as far as weight loss is concerned. The general weight loss also decreased with increasing melting temperature from 1600 °C to 1800 °C. At 1600 °C and 1700 °C, the amount of FBR-Si added played a major role in reducing the material loss, with an approximately 40% reduction in weight loss from 20 wt.% to 30 wt.% FBR-Si addition. However, at 1800 °C, the effect of increasing the FBR-Si amount from 20 wt.% to 30 wt.% was only about 20%, showing that at higher temperatures, the material loss is reduced regardless of the quantity of FBR-Si additives. The material loss can be attributed to loss of moisture which vaporizes upon heating as well the vaporization of volatile organic polymer materials at elevated temperatures. Another major contributor to the mass loss is in the form of SiO gas due to the reaction of molten Si with the solid SiO₂ (on the surface of Si particles or the adjacent slag formed) at temperatures beyond the melting point of Si, according to Equation (6):



Another mechanism for the mass loss may be the interaction of SiO₂ with the graphite crucible and the following reactions, (7)–(9), show the interaction of the graphite crucible at elevated temperatures. The schematic for the interaction is shown in Figure 10. The point of interaction is indicated by the dotted red circle.



Considering the graphite crucible and its contents, we have different phases and a couple of heterogeneous simultaneous reactions occurring, such as:



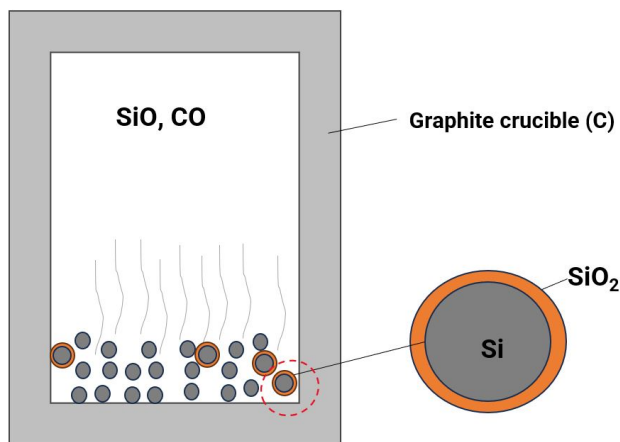


Figure 10. Interaction of graphite crucible with the sample.

And in the system, the following reaction in Equation (10) yields Si metal:



The reduced mass loss with increasing temperature can be attributed to silicon recovery (from the oxide surface of the Si particles) at elevated temperatures due to the presence of C (graphite) in the system. In short, at higher temperatures, there is lower SiO gas loss and O loss occurs more via CO gas generation and leaving the sample.

3.4. Features of Melted Samples and Microstructural Study

The melting of the samples at 1600 °C and 1700 °C improved with increasing FBR silicon content, as seen in Figure 11. At 40 wt.% FBR and at 1700 °C, there was complete melting of the samples. The SEM images show how the FBR silicon granules act as nuclei for the melting process, indicated by the circular clusters progressively growing into one big silicon powder matrix. Increasing the temperature between 1600 °C and 1800 °C also improved the melting. The oxidation of the surface could also be observed from both visual inspection and micrographs from SEM as indicated by red circles and the brownish coloration. Elemental mapping by EDS also confirmed the surface oxidation in the silicon matrix. The general observation was that there is less oxidation as the amount of FBR silicon granules increased. This is because the fine silicon kerf powder is more susceptible to oxidation compared to solid granules. The melting improved, as expected, as the temperature increased from 1600 °C to 1800 °C as shown in Figures 11 and 12, with complete melting being observed throughout the crucibles at 1800 °C even without any additives. At lower temperatures (1600 °C and 1700 °C) and lower FBR-Si additions, the melting was incomplete, with patches of molten silicon and a lot of surface oxidation. Only the bottom parts of the crucible had sufficient melting under these conditions. The rate of surface oxidation is lower as we increase temperature to ultrahigh values (>1700 °C), and thus there is more complete melting of the Si metal and less formation of SiO₂ at the surface of the molten metal. Cracking was observed in all of the melted samples regardless of the conditions of temperature and quantity of additives. This crack formation indicates that melting occurred and hence good contact of molten silicon with the crucible walls was obtained. Eventually, the volume increase upon solidification of silicon causes crack formation. It is worth noting that the cracks pose difficulties in surface analysis by methods such as GDMS and SIMS where sputtering is required, and the homogeneity of the surface is of high importance.

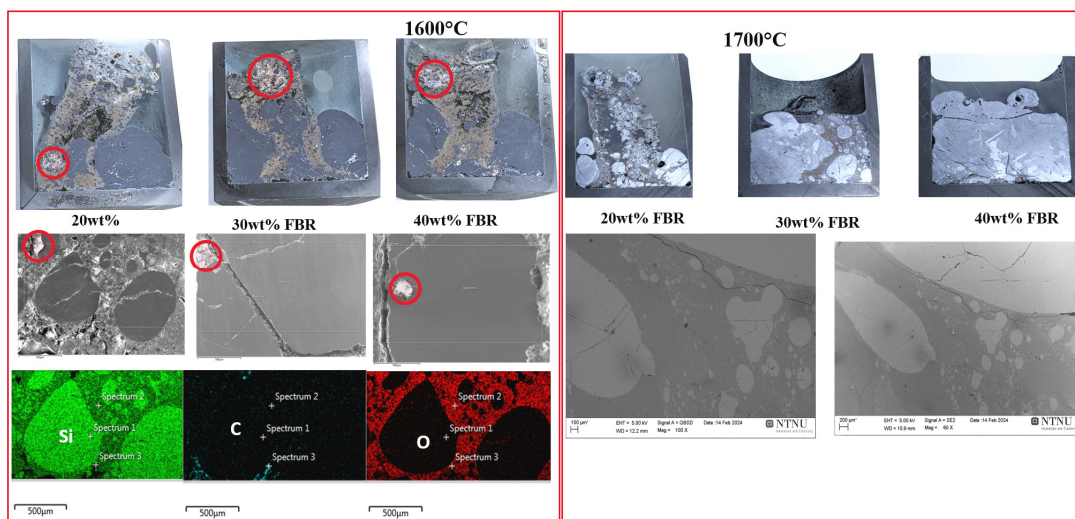


Figure 11. Cross sections of crucibles after melting of samples at 1600 °C and 1700 °C.

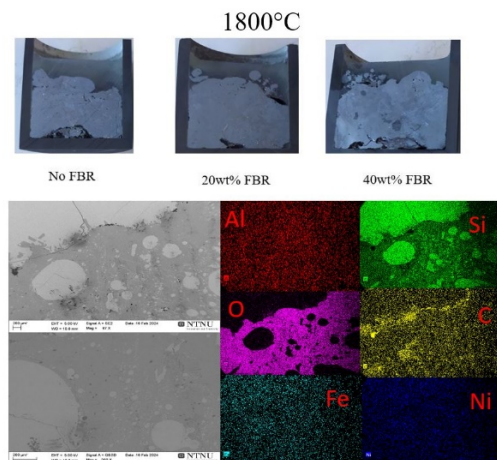


Figure 12. Cross sections of crucibles after melting of samples at 1800 °C.

Figure 12 also shows that at 1800 °C, there is less visible surface oxidation and relatively uniform melting even though the same residence time was used. Though less visible with the naked eye, examination using EDS shows that surface oxidation still occurs under the given conditions. The distribution of the main metallic impurities is also shown and agrees with the results from GDMS, where Al is the main metallic impurity, followed by Ni and Fe. A conclusion can thus be made that at higher temperatures like 1800 °C and above no FBR silicon addition is necessary.

Impurity Distribution Analysis by Secondary-Ion Mass Spectrometry (SIMS)

Analysis of the main metallic impurity (Al) as well as C and O was conducted using the SIMS depth profile regime. This was carried out to analyze the distribution of the impurities from the surface into the sample after inductive melting. The sensitivity of SIMS to very low concentrations (up to ppb) makes it very useful for analyzing high purity materials like solar-grade silicon. In the present contribution, the SIMS measurements were performed with a Cameca IMS 7f microanalyzer with a primary beam of 10 keV O_2^+ and 15 keV Cs^+ for the detection of Al and O/C, respectively. The SIMS intensity-to-concentration calibration was performed using ion-implanted reference samples, while the depth conversion of the recorded profiles was performed by measuring the sputtered crater depth and assuming a constant erosion rate. The typical concentration versus depth profiles of C, O, Al and Ca, as measured by SIMS, are shown in Figure 13a–d, respectively.

It is seen that there is an enhanced concentration of all measured elements near the surface. For all elements, the concentrations gradually decrease with the depth and stabilize at depths more than $\sim 4 \mu\text{m}$. The width of this transition region can be related to the surface roughness. Furthermore, it can be seen that the bulk concentrations of both the C and O are lower for the FBR+KLW (1800°C) samples, while the Al content in this sample is higher as compared to both no-FBR and FBR (1800°C) + KLW (1700°C) samples.

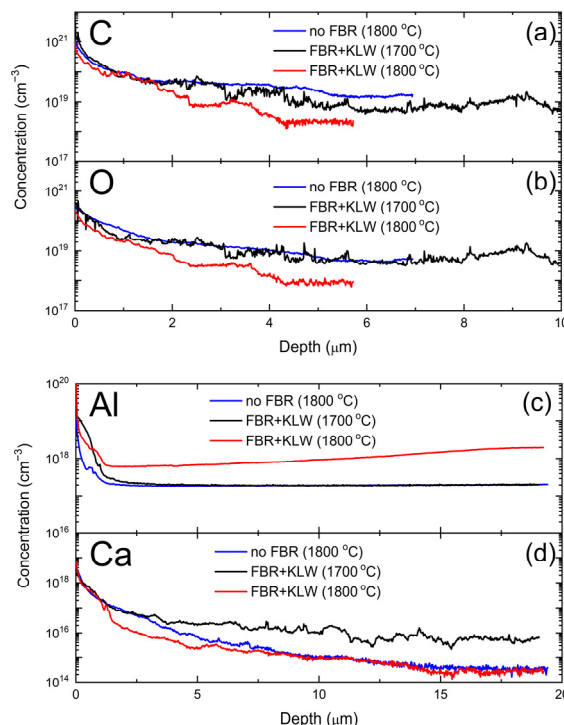


Figure 13. The concentration versus depth profiles, as measured by SIMS, of (a) C, (b) O (c) Al and (d) Ca in the melted samples at 1700°C and 1800°C .

The existence of a tiny $\text{CaO}-\text{Al}_2\text{O}_3-\text{SiO}_2$ slag phase on the surface of the produced Si melt is confirmed by SIMS surface measurements in Figure 13 and supports the above observations and discussions for Ca and Al removal described above. The concentration C_i in ppmw is given by Equation (11):

$$C_i [\text{ppmw}] = C_i [\text{atoms}/\text{cm}^3] \cdot M_i / N_A \cdot \rho_{\text{Si}} \quad (11)$$

where M_i is the atomic weight of the individual elements, N_A is the Avogadro constant and ρ_{Si} is the density of liquid Si. In addition to the Ca and Al concentrations detected and measured by GDMS in Table 1, the SIMS measurements for the sample at 1700°C show that at the surface of the melt, there is approximately 0.2 wt.% O and 0.8 wt.% C from the oxidation as well as the interaction with the graphite crucible as described in Figure 10.

4. Conclusions

A study on the combined effect of single-acid leaching on KLW purification with further melting was carried out and evaluated. In addition, a couple of characterization techniques were used. The main conclusions are summarized as follows:

- After leaching and induction melting at 1600°C , 1700°C and 1800°C , the best overall impurity removal efficiency was found to be 93% with a purity of 99.92% (3 N) from the GDMS measurements. This requires an additional directional solidification step to get to solar grade, or alternatively, it can be used directly as an alloying element.

2. The behavior of the impurity elements with regards to their reactivity and volatility during the melting of Si kerf particles showed that a significant portion of volatile elements (Mn, Mg, P and Ga) evaporated, while more reactive metals (Ca and Al) formed a slag phase, and the less reactive metals (Fe, Ni, Ti and Cu) ended up in the recovered Si.
3. The melting of powder KLW was accompanied by material losses between 2 wt.% and 10 wt.%, and this decreased with an increasing amount of FBR silicon granules added or increasing temperature, yielding higher Si recovery from the kerf.
4. It was observed that melting improved as the temperature increased from 1600 °C to 1800 °C, with complete melting being observed throughout the crucibles at 1800 °C even without any additives. The impurities are mainly concentrated at the surface and decrease with depth and stabilize at a depth of >~4 μm.
5. It was concluded that if optimized, the combined treatment of single-acid leaching and inductive melting with the addition of granular FBR silicon has great potential for the recycling of KLW to solar cells and similar applications.

Author Contributions: Conceptualization, T.M. and J.S.; methodology, T.M. and J.S.; software, T.M., A.G., A.A. and J.S.; validation, T.M., A.G., A.A. and J.S.; formal analysis, T.M., A.G. and A.A.; investigation, T.M., A.G. and A.A.; resources, J.S.; writing—original draft preparation, T.M.; writing—review and editing, T.M., A.G., A.A. and J.S.; visualization, T.M.; supervision, J.S.; project administration, J.S.; funding acquisition, J.S. All authors have read and agreed to the published version of the manuscript.

Funding: This research was funded by Research Centre for Sustainable Solar Cell Technology (FME SuSolTech) cosponsored by the Norwegian Research Council and industry partners, grant by project number 257639.

Data Availability Statement: The data for our findings are provided in the manuscript and the raw data supporting the conclusions of this article will be made available by the corresponding author upon reasonable request.

Acknowledgments: We would like to acknowledge Tyke Naas and Erik Enebakk from REC Solar for their invaluable contribution to this work.

Conflicts of Interest: The authors declare no conflicts of interest.

References

1. Braga, A.F.B.; Moreira, S.P.; Zampieri, P.R.; Bacchin, J.M.G.; Mei, P.R. New processes for the production of solar-grade polycrystalline silicon: A review. *Sol. Energy Mater. Sol. Cells* **2008**, *92*, 418–424. [[CrossRef](#)]
2. Obeidat, F. A comprehensive review of future photovoltaic systems. *Sol. Energy* **2018**, *163*, 545–551. [[CrossRef](#)]
3. Parida, B.; Iniyian, S.; Goic, R. A review of solar photovoltaic technologies. *Renew. Sustain. Energy Rev.* **2011**, *15*, 1625–1636. [[CrossRef](#)]
4. Kabir, E.; Kumar, P.; Kumar, S.; Adelodun, A.A.; Kim, K.H. Solar energy: Potential and future prospects. *Renew. Sustain. Energy Rev.* **2018**, *82*, 894–900. [[CrossRef](#)]
5. Hachichi, K.; Lami, A.; Zemmouri, H.; Cuellar, P.; Soni, R.; Ait-Amar, H.; Drouiche, N. Silicon Recovery from Kerf Slurry Waste: A Review of Current Status and Perspective. *Silicon* **2018**, *10*, 1579–1589. [[CrossRef](#)]
6. Bye, G.; Ceccaroli, B. Solar grade silicon: Technology status and industrial trends. *Sol. Energy Mater. Sol. Cells* **2014**, *130*, 634–646. [[CrossRef](#)]
7. Chigondo, F. From Metallurgical-Grade to Solar-Grade Silicon: An Overview. *Silicon* **2018**, *10*, 789–798. [[CrossRef](#)]
8. Cowern, N.E.B. 1. Silicon-based photovoltaic solar cells. In *Functional Materials for Sustainable Energy Applications*; Kilner, J.A., Skinner, S.J., Irvine, S.J.C., Edwards, P.P., Eds.; Woodhead Publishing Limited: Cambridge, UK, 2012; pp. 3–22e. [[CrossRef](#)]
9. Blömeke, S.; Arafat, R.; Yang, J.; Mai, J.-P.; Cerdas, F.; Herrmann, C. Environmental assessment of silicon kerf recycling and its benefits for applications in solar cells and Li-ion batteries. *Procedia CIRP* **2023**, *116*, 179–184. [[CrossRef](#)]
10. Chen, G.; Li, W.; Huang, L.; Tang, L.; Luo, X. Al₂O₃ and CaO as sintering aids: A strategy to remove impurity boron and SiO₂ surface-layer of diamond wire saw silicon waste. *Sep. Purif. Technol.* **2021**, *270*, 118823. [[CrossRef](#)]
11. Vazquez-Pufleau, M.; Chadha, T.P.; Yablonsky, G.; Biswas, P. Carbon elimination from silicon kerf: Thermogravimetric analysis and mechanistic considerations. *Sci. Rep.* **2017**, *7*, 40535. [[CrossRef](#)]
12. Li, J.; Lin, Y.; Wang, F.; Shi, J.; Sun, J.; Ban, B.; Liu, G.; Chen, G. Progress in recovery and recycling of kerf loss silicon waste in photovoltaic industry. *Sep. Purif. Technol.* **2021**, *254*, 117581. [[CrossRef](#)]

13. Yang, F.; Yu, W.; Rao, Z.; Wie, P.; Jiang, W.; Chen, H. A new strategy for de-oxidation of diamond-wire sawing silicon waste via the synergistic effect of magnesium thermal reduction and hydrochloric acid leaching. *J. Environ. Manag.* **2022**, *317*, 115424. [[CrossRef](#)] [[PubMed](#)]
14. Yang, H.L.; Liu, I.T.; Liu, C.E.; Lan, C.W. Recycling and reuse of kerf-loss silicon from diamond wire sawing for photovoltaic industry. *Waste Manag.* **2019**, *84*, 204–210. [[CrossRef](#)] [[PubMed](#)]
15. Zou, Q.; Huang, L.; Chen, W.; Chen, G.; Li, Y.; Li, M.; Zhang, C.; Luo, X. Recycling of silicon from waste PV diamond wire sawing silicon powders: A strategy of Na_2CO_3 -assisted pressure-less sintering and acid leaching. *Waste Manag.* **2023**, *168*, 107–115. [[CrossRef](#)] [[PubMed](#)]
16. Chen, G.; Li, Y.; Huang, L.; Peng, J.; Tang, L.; Luo, X. Recycling silicon kerf waste: Use cryolite to digest the surface oxide layer and intensify the removal of impurity boron. *J. Hazard. Mater.* **2022**, *423*, 126979. [[CrossRef](#)] [[PubMed](#)]
17. Hu, Z.; Wang, G.; Li, J.; Tan, Y.; Liu, Y.; Li, P. Recycling of diamond-wire sawing silicon powder by direct current assisted directional solidification. *Waste Manag.* **2023**, *157*, 190–198. [[CrossRef](#)] [[PubMed](#)]
18. Li, X.; Lv, G.; Ma, W.; Li, T.; Zhang, R.; Zhang, J.; Li, S.; Lei, Y. Review of resource and recycling of silicon powder from diamond-wire sawing silicon waste. *J. Hazard. Mater.* **2022**, *424*, 127389. [[CrossRef](#)] [[PubMed](#)]
19. Zenodo, CABRISS Project (H2020). Available online: <https://zenodo.org/records/815891> (accessed on 12 June 2024).
20. Kong, J.; Wei, D.; Xing, P.; Jin, X.; Zhuang, Y.; Yan, S. Recycling high-purity silicon from diamond-wire saw kerf slurry waste by vacuum refining process. *J. Clean. Prod.* **2021**, *286*, 124979. [[CrossRef](#)]
21. Ultra Low-Carbon Solar Alliance. Available online: <https://ultralowcarbonsolar.org/blog/q-and-a-series-david-verdu-rec-group/> (accessed on 12 June 2024).
22. Bao, Q.; Wu, J.; Wie, W.; Ma, W. Melting Behavior of Diamond Wire Saw Silicon Powder after Acid Leaching Treatment during Recycling Process. *Silicon* **2024**, *16*, 3383–3393. [[CrossRef](#)]
23. Yang, S.; Wei, K.; Ma, W.; Xie, K.; Wu, J.; Lei, Y. Kinetic mechanism of aluminum removal from diamond wire saw powder in HCl solution. *J. Hazard. Mater.* **2019**, *368*, 1–9. [[CrossRef](#)]
24. Liddell, K.C. Shrinking core models in hydrometallurgy: What students are not being told about the pseudo-steady approximation. *Hydrometallurgy* **2005**, *79*, 62–68. [[CrossRef](#)]
25. Raschman, P.; Popović, L.; Fedoročková, A.; Kyslytsyna, M.; Sučík, G. Non-porous shrinking particle model of leaching at low liquid-to-solid ratio. *Hydrometallurgy* **2019**, *190*, 105151. [[CrossRef](#)]
26. Faraji, F.; Alizadeh, A.; Rashchi, F.; Mostoufi, N. Kinetics of leaching: A review. *Rev. Chem. Eng.* **2022**, *38*, 113–148. [[CrossRef](#)]
27. Safarian, J.; Tangstad, M. Kinetics and mechanism of phosphorus removal from silicon in vacuum induction refining. *High Temp. Mater. Process.* **2012**, *31*, 73–81. [[CrossRef](#)]
28. Safarian, J.; Tangstad, M. Vacuum refining of molten silicon. *Metall. Mater. Trans. B Process Metall. Mater. Process. Sci.* **2012**, *43*, 1427–1445. [[CrossRef](#)]

Disclaimer/Publisher's Note: The statements, opinions and data contained in all publications are solely those of the individual author(s) and contributor(s) and not of MDPI and/or the editor(s). MDPI and/or the editor(s) disclaim responsibility for any injury to people or property resulting from any ideas, methods, instructions or products referred to in the content.